

Atf İçin: Yıldırım H, Çakır R, 2022. Polar Olmayan ZnO/BeMgZnO Kuantum Kuyularında Altbantlar Arası Geçişler: Fiziksel Boyut, Konsantrasyon ve Donör Seviyesinin Etkileri. İğdır Üniversitesi Fen Bilimleri Enstitüsü Dergisi, 12(4): 2113 - 2128.

To Cite: Yıldırım H, Çakır R, 2022. Intersubband Transitions in Nonpolar ZnO/BeMgZnO Quantum Wells: Effects of Physical Dimension, Concentration and Donor Level. Journal of the Institute of Science and Technology, 12(4): 2113 - 2128.

Polar Olmayan ZnO/BeMgZnO Kuantum Kuyularında Altbantlar Arası Geçişler: Fiziksel Boyut, Konsantrasyon ve Donör Seviyesinin Etkileri

Hasan YILDIRIM^{1*}, Raşit ÇAKIR²

ÖZET: Polar ve semipolar yönlerde büyütülen BeMgZnO bariyer tabakaları üzerindeki ZnO kuyu katmanlarının polarizasyon özellikleri araştırıldı. Gevşemiş ve gerilmiş bariyer katmanların durumları göz önünde bulunduruldu. Arayüzlerdeki polarizasyon farkının, kuyu tabakası içinde 8 MV cm^{-1} büyüklüğünde yerleşik bir elektrik alanına yol açtığı bulundu. Polar olmayan ZnO/BeMgZnO kuantum kuyuları, altbantlar arası geçişler açısından incelendi. Hesaplamalar Be ve Mg konsantrasyonlarını sırasıyla 0.18 ve 0.5'e kadar kapsamaktadır. 50 ila 700 meV arasında değişen altbantlar arası geçiş (ISBT) enerjilerinin mümkün olduğu bulundu. Bariyer kalınlığının ISBT enerjileri üzerindeki etkisi incelendi. Sonuçlar, enerjilere kıyasla ISBT enerjilerinde önemsiz değişiklikler olduğunu göstermektedir.

Anahtar Kelimeler: ZnO, BeMgZnO, altbantlar arası geçişler, kuantum kuyuları

Intersubband Transitions in Nonpolar ZnO/BeMgZnO Quantum Wells: Effects of Physical Dimension, Concentration and Donor Level

ABSTRACT: Polarization properties of ZnO well layers on BeMgZnO barrier layers grown in polar and semipolar orientations have been investigated. Cases of relaxed and strained barrier layers are considered. It is found that the polarization difference at the interfaces leads to a built-in electric field inside the well layer as much as 8 MV cm^{-1} in magnitude. Nonpolar ZnO/BeMgZnO quantum wells have been studied in terms of intersubband transitions. The calculations have covered Be and Mg concentrations up 0.18 and 0.5, respectively. It has been found that intersubband transition (ISBT) energies ranging from 50 to 700 meV are possible. The effect of barrier thickness on the ISBT energies has been studied. The results indicate insignificant changes in ISBT energies compared to the energies.

Keywords: ZnO, BeMgZnO, intersubband transitions, quantum wells

¹Hasan YILDIRIM ([Orcid ID:0000-0002-7436-7759](https://orcid.org/0000-0002-7436-7759)), Karabük University, Faculty of Health Sciences, Department of Occupational Health and Safety, Karabük, Türkiye

²Raşit ÇAKIR ([Orcid ID:0000-0002-7104-9069](https://orcid.org/0000-0002-7104-9069)), Recep Tayyip Erdoğan University, Faculty of Arts and Sciences, Department of Physics, Rize, Türkiye

***Sorumlu Yazar/Corresponding Author:** Raşit ÇAKIR, e-mail: rasit.cakir@erdogan.edu.tr

INTRODUCTION

ZnO is a wideband gap material with a band gap of 3.3 eV. Low dimensional structures of ZnO, together with its several alloys, such as ZnCdO, ZnMgO, and ZnBeO, have been studied (Ryu et al., 2006; Sadofev et al., 2007; Lange et al., 2011; Park et al., 2014; Pearton and Ren, 2014; Shteplyuk et al., 2015; Zhao et al., 2015; Orphal et al., 2017; Zúñiga-Pérez, 2017; Özgür et al., 2018; Liu et al., 2019; Sirkeli and Hartnagel, 2019; Yildirim, 2019; Pietrzyk et al., 2020; Park, 2020; Hong and Park, 2021; Meng et al., 2021; Yıldırım, 2021; Zhang, et al., 2022). It has been shown that ZnCdO/ZnO quantum wells are capable of emitting in the visible spectral range (Sadofev et al., 2007; Lange et al., 2011; Zúñiga-Pérez, 2017; Pietrzyk et al., 2020). Recent calculations on the intersubband transitions (ISBTs) in the ZnCdO/ZnO quantum wells show that these quantum wells yield in principle ISBT energies in THz and MIR ranges (Yildirim, 2019; Yıldırım, 2021). ZnO/ZnMgO quantum wells with a conduction band offset up to 0.7 eV offer ISBT energies reaching to the NIR region (Orphal et al., 2017). Recently, for instance, non-polar ZnO/ZnMgO quantum wells have been reported to have a THz electroluminescence (around 8.5 THz) based on intersubband transitions for the first time (Meng et al., 2021). Alloying ZnO with Be extends its band gap to the UV range (Ryu et al., 2006). In fact, an ultraviolet light emitting diode based on a BeZnO/ZnO active layer was fabricated (Ryu et al., 2006).

However, the binary materials BeO, CdO, and MgO have restricted solubility in ZnO, either because of having a different stable phase, like the rocksalt phase in the case of CdO and MgO, or having a much different covalent radius, like in the case of BeO (Toporkov et al., 2016; Zúñiga-Pérez, 2017; Zhang, et al., 2022). These parameters lead to a phase segregation in the ternary compounds of CdO, BeO and MgO with ZnO (Toporkov et al., 2016; Zúñiga-Pérez, 2017; Zhang, et al., 2022). To overcome such issues, a quaternary alloy BeMgZnO has been suggested (Toporkov et al., 2014; Toporkov et al., 2016). Achievement of fabrication of Schottky barriers on BeMgZnO/ZnO heterostructures with a high crystalline quality and a high two dimensional electron gas has been reported recently (Ullah et al., 2017; Ding et al., 2018).

To the best of our knowledge, studies on the optical and electronic properties of ZnO/Be_xMg_yZn_{1-x-y}O quantum wells are lacking in the literature. We believe that a thorough calculation of the polarization and the strain properties of the ZnO/ Be_xMg_yZn_{1-x-y}O quantum wells and the determination of the possible energy ranges due to the transitions of the electrons within the conduction band will contribute to the area of the applications of the ZnO-based heterostructures. We begin with the polarization properties of ZnO well layers on Be_xMg_yZn_{1-x-y}O barrier layers as a function of x and y . We consider two cases: the case of relaxed Be_xMg_yZn_{1-x-y}O layers and the case of strained Be_xMg_yZn_{1-x-y}O layers. Then, we discuss the built-in electric field inside the ZnO/Be_xMg_yZn_{1-x-y}O quantum wells oriented in polar and semipolar axes for both cases. Finally, we present the results of our calculations on the ISBT energies of the nonpolar ZnO/Be_xMg_yZn_{1-x-y}O quantum wells in the cases I and II. Our calculation includes the many-body effects and the effects of the changes in the Be and Mg concentrations, the physical dimension of the structure and the doping level.

MATERIALS AND METHODS

Polarization properties of polar and semipolar quantum wells

A wurtzite ZnO/Be_xMg_yZn_{1-x-y}O quantum well can be formed basically by squeezing the ZnO well layer between two Be_xMg_yZn_{1-x-y}O layers. A square well potential is established along the structure due to the special alignment of the band gaps of the constituting materials. But, these wurtzite materials possess spontaneous and piezoelectric polarization properties and the difference between the total

polarization of each material at the interfaces of the structure creates a built-in electric field along it (Zúñiga-Pérez, 2017; Zhang, et al., 2022). Therefore, the square potential energy profile of the quantum well is distorted and bent. Wurtzite ZnO/Be_xMg_yZn_{1-x-y}O quantum wells yield such bent potential energy profiles when they are grown along the polar or semipolar axis.

The piezoelectric polarization inside a well or barrier layer mainly depends on the strain present in it. We will consider two cases in this work: I) a thick BeMgZnO barrier layer relaxed on a substrate and II) a thin BeMgZnO barrier layer strained on a substrate. We do not deal with specifically a lattice-matching condition between the ZnO substrate and the BeMgZnO barrier layer. Therefore, the barrier layers in general will be strained. The case I models a quantum well with barriers assumed to be thick enough to be relaxed and strain-free. The case II models a quantum well with barriers assumed thin to include the strain. The first case yields only a spontaneous polarization inside the BeMgZnO barrier layer but it allows a piezoelectric and a spontaneous polarization inside the ZnO well layer. The second case yields both polarization types inside the barrier layer but it allows only a spontaneous polarization inside the well layer. Energy considerations limit the thickness of a layer to be grown pseudomorphically on a substrate (Harrison and Valavanis, 2016). There is a critical thickness for the layer above which it will have defects and imperfections. The critical thickness of a Be_xMg_yZn_{1-x-y}O layer on a substrate will mainly depend on the concentrations of its alloys. We will assume that the Be_xMg_yZn_{1-x-y}O barrier layer is grown on a ZnO substrate. A simple formula to calculate the critical thickness L_c of a layer with a lattice constant a_0 grown on a substrate with a lattice constant a_s is given by (Holec et al., 2007; Shein et al., 2007; Harrison and Valavanis, 2016)

$$L_c = \frac{a_0}{\sqrt{2\pi f}} \frac{1-v/4}{1+v} \left[\ln \left(\frac{\sqrt{2}L_c}{a_0} \right) + 1 \right] \quad (1)$$

where v is the Poisson ratio and f is the misfit between the substrate and the layer and it is given by

$$f = \left| \frac{a_s - a_0}{a_0} \right| \quad (2)$$

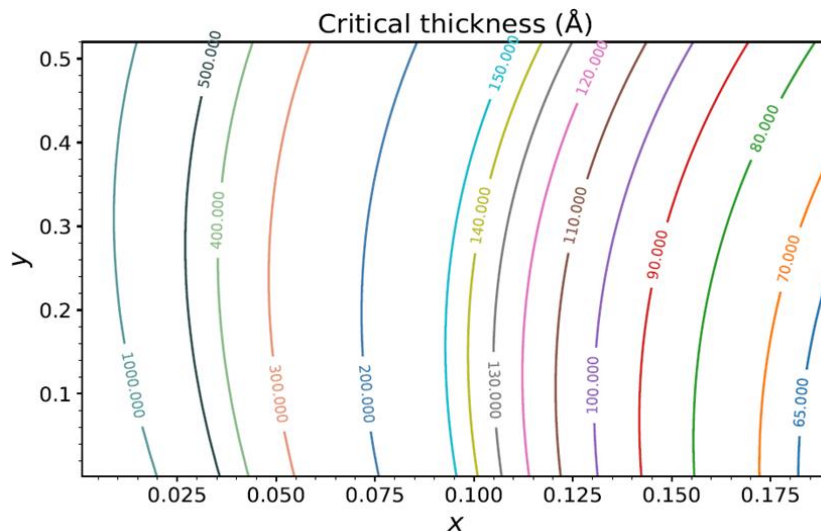


Figure.1. Critical thickness values of a Be_xMg_yZn_{1-x-y}O layer strained on a ZnO substrate as a function of the Be and Mg concentrations

Figure.1 depicts the critical thickness values as a function of both x and y . The material parameters used in the calculation are listed in Table 1. Those of the quaternary alloy, Be_xMg_yZn_{1-x-y}O, except for the lattice constants a_0 , c_0 and the band gap E_g , are calculated by applying an expression which uses a linear combination of the binary material parameters. A nonlinear expression (Toporkov et al., 2016) as

given in Equation (2) is applied to each of a_0 , c_0 and E_g . The bowing parameters of these quantities are listed in Table 2. According to Figure.1, the L_c values go up as the Mg concentration of the quaternary alloy increases. This is reasonable as the binary MgO has a lattice constant very close to that of the binary ZnO. However, the L_c values quickly drop with the increasing Be concentration: L_c reaches to the values as low as $\approx 65 \text{ \AA}$ around $x = 0.19$. So, we can say that the large difference between the lattice constants of the binaries BeO and ZnO may not allow thick BeMgZnO layers to be grown pseudomorphically on a ZnO substrate.

Table 1. Material parameters of the binary compounds that are used in the calculations

Parameter (Unit)	Meaning	BeO	MgO	ZnO	Ref(s).
a_0 (Å)	Lattice constant	2.72	3.32	3.3	(Toporkov et al., 2016)
a_{ct} (eV)	Deformation potential	2.165	3.98	2.165	(Yan et al., 2012; Wagner et al., 2013)
a_{cz} (eV)	Deformation potential	1.705	0.975	1.705	(Yan et al., 2012; Wagner et al., 2013)
c_0 (Å)	Lattice constant	4.393	5.056	5.285	(Toporkov et al., 2016)
C_{11} (GPa)	Elastic constant	461	205	209.7	(Özgür et al., 2005; Duman et al., 2009; Jang and Chichibu, 2012)
C_{12} (GPa)	Elastic constant	126	80	121.1	(Özgür et al., 2005; Duman et al., 2009; Jang and Chichibu, 2012)
C_{13} (GPa)	Elastic constant	88	88	105.1	(Özgür et al., 2005; Duman et al., 2009; Jang and Chichibu, 2012)
C_{33} (GPa)	Elastic constant	491	222	210.9	(Özgür et al., 2005; Duman et al., 2009; Jang and Chichibu, 2012)
C_{44} (GPa)	Elastic constant	147	58	42.47	(Özgür et al., 2005; Duman et al., 2009; Jang and Chichibu, 2012)
e_{15} (C m ⁻²)	Piezoelectric constant	-0.174	-0.36	-0.37	(Özgür et al., 2005; Duan et al., 2008; Jang and Chichibu, 2012)
e_{31} (C m ⁻²)	Piezoelectric constant	-0.317	-0.78	-0.62	(Özgür et al., 2005; Duan et al., 2008; Jang and Chichibu, 2012)
e_{33} (C m ⁻²)	Piezoelectric constant	0.56	0.14	0.96	(Özgür et al., 2005; Duan et al., 2008; Jang and Chichibu, 2012)
$\epsilon_{\infty,z}$	Dielectric constant	3	3.02	3.78	(Özgür et al., 2005; Duman et al., 2009; Schleife et al., 2009)
$\epsilon_{s,z}$	Dielectric constant	7.73	9.87	8.91	(Özgür et al., 2005; Duman et al., 2009; Schleife et al., 2009)
E_g (eV)	Band gap	10.2	5.87	3.43	(Toporkov et al., 2016)
m_z^*	Effective mass	0.58	0.42	0.25	(Xu and Ching, 1993; Schleife et al., 2009; Jang and Chichibu, 2012)
P_{SP} (C m ⁻²)	Spontaneous polarization	-0.045	-0.08	-0.053	(Ullah, 2017; Jang and Chichibu, 2012)

Table 2. The bowing parameters of the lattice constants and the energy band gap

Bowing parameter	a_0 (Å)	c_0 (Å)	E_g (eV)
b_{BeZnO}	-0.043	-0.043	6.94
b_{MgZnO}	0.061	-0.172	0.277
b_{xy}	-0.14	0.427	-2.79

We have calculated the polarization properties of the well and barrier layers for a ZnO/Be_xMg_yZn_{1-x-y}O quantum well in the cases I and II. We consider the polar and semipolar growths for the well. The expressions for the piezoelectric polarization P_{PZ} and the spontaneous polarization P_{SP} written for the polar and semipolar axes are taken from Refs. (Romanov et al., 2006; Grundmann and Zúñiga-Pérez, 2015; Yıldırım, 2021). Figure.2 (a) and (b) depict the total polarization inside the ZnO well layer of the quantum well for the polar and semipolar orientations, respectively, in the case I. The barrier layer is relaxed so its polarization property is governed by its spontaneous polarization. However, the well layer admits both the piezoelectric and spontaneous polarizations as it is strained. According to the panel (a), $P_{T,W}$ values go up and finally become positive as the Be concentration increases. That means the introduced piezoelectric polarization inside the well layer is positive as the P_{SP} of ZnO the layer is

-0.053 C m^{-2} . This is expected because the compressive strain inside the ZnO layer becomes larger as the the Be concentration increases and that leads to a positive piezoelectric polarization inside the layer. Note that the $P_{T,W}$ values are less sensitive to the changes in the Mg concentration. In the case of the semipolar growth, $P_{T,W}$ is totally negative for all values of x and y as shown in the panel (b). That means P_{PZ} becomes negative with this choice of the growth axis. Besides, its change with the Mg concentration is noticeable: it goes down with the increasing y values.

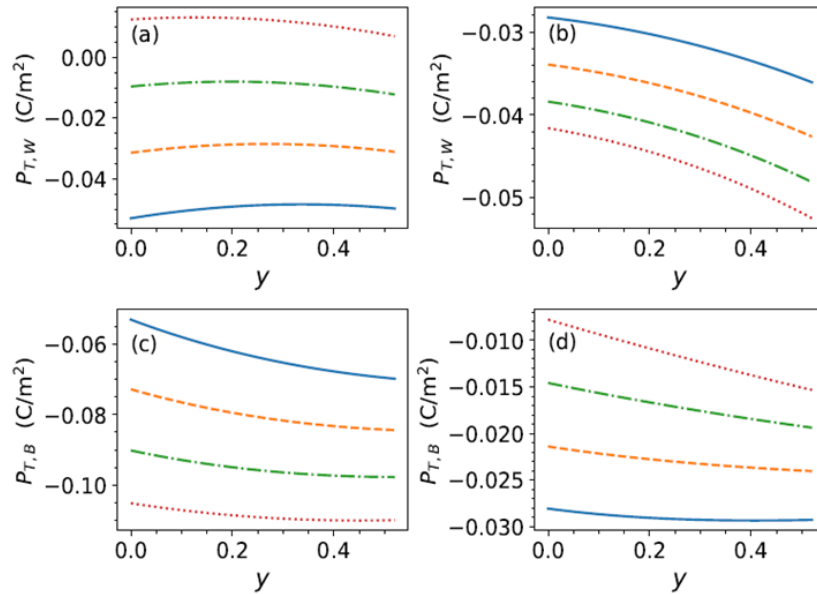


Figure.2. The total polarization in a ZnO layer strained on a relaxed $\text{Be}_x\text{Mg}_y\text{Zn}_{1-x-y}\text{O}$ layer as a function the Mg concentration, y : (a) when the growth axis is the polar axis and (b) the semipolar axis. The total polarization in a $\text{Be}_x\text{Mg}_y\text{Zn}_{1-x-y}\text{O}$ layer strained on a ZnO substrate as a function the Mg concentration, y : (c) when the growth axis is the polar axis and (d) the semipolar axis. The solid, dashed, dashed-dotted, and dotted lines stand for $x = 0, 0.06, 0.12,$ and $0.18,$ respectively, in all panels

The panels (c) and (d) of Figure.2 present the results for the polar and semipolar orientations, respectively, in the case II. The barrier layer is under a tensile strain but the well layer is strain free. That causes a negative piezoelectric polarization inside the barrier layer and makes P_{PZ} increase in the negative direction. Therefore $P_{T,B}$ goes down as x increases. On the other hand, the semipolar growth reverses this trend and $P_{T,B}$ goes up as x increases. The increasing Mg concentration reduces the total polarization inside the barrier layer in both orientations.

The built-in electric field (Harrison and Valavanis, 2016) F_{bi} inside a well layer of a polar quantum well is proportional to the polarization difference at the interfaces of the structure. Therefore, the polarization difference at the interface of the ZnO and $\text{Be}_x\text{Mg}_y\text{Zn}_{1-x-y}\text{O}$ layers has been calculated and the results are plotted in Figure.3. The panels (a) and (b) show the results for the polar and semipolar orientations, respectively, in the case I. Note that the $\text{Be}_x\text{Mg}_y\text{Zn}_{1-x-y}\text{O}$ layer possesses only a spontaneous polarization as it is assumed to be relaxed over the substrate. ΔP in the case of the polar growth is positive and it becomes larger as x increases because of the negative polarization of the $\text{Be}_x\text{Mg}_y\text{Zn}_{1-x-y}\text{O}$ layer. On the contrary, ΔP in the case of the semipolar growth changes sign with the decreasing Be concentration. According to the panel (b), it is possible that there is a zero polarization difference around $x = 0$ for all y . The panels (c) and (d) show the results for the polar and semipolar orientations, respectively, in the case II. ΔP in the case of the polar growth is positive for all x and y . This is because

$P_{T,B}$ is more negative than $P_{T,W}$. While ΔP is still negative nearly for all x and y for the semipolar growth, it becomes almost zero for $x = 0$.

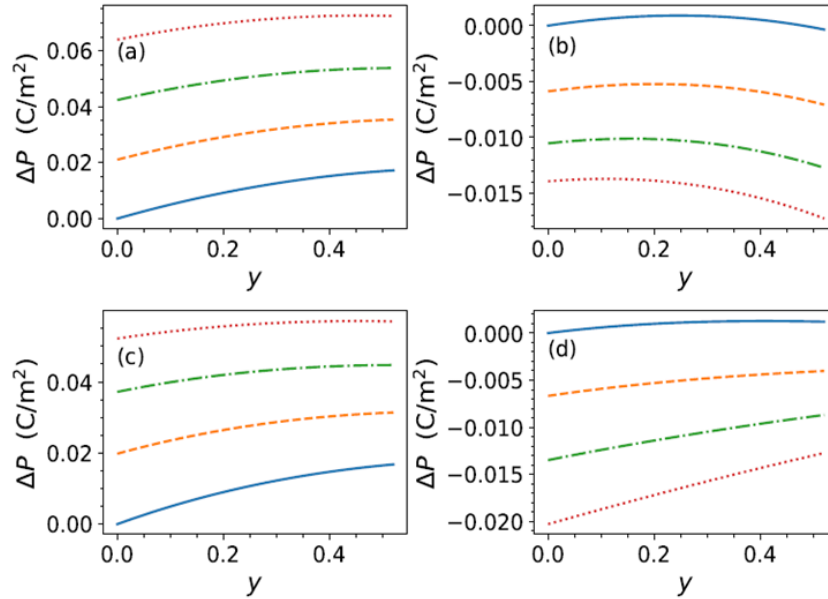


Figure.3. The polarization difference between those of a relaxed $\text{Be}_x\text{Mg}_y\text{Zn}_{1-x-y}\text{O}$ barrier layer and a ZnO well layer strained on it as a function the Mg concentration, y : (a) when the growth axis is the polar axis and (b) the semipolar axis.

The polarization difference between those of a ZnO well layer and $\text{Be}_x\text{Mg}_y\text{Zn}_{1-x-y}\text{O}$ barrier layer strained on a ZnO substrate as a function the Mg concentration, y : (c) when the growth axis is the polar axis and (d) the semipolar axis. The solid, dashed, dashed-dotted, and dotted lines stand for $x = 0, 0.06, 0.12,$ and $0.18,$ respectively, in all panels

Built-in electric field inside polar and semipolar quantum wells

We have calculated the built-in electric field (Harrison and Valavanis, 2016), F_{bi} , inside the well layer of a $30 - \text{\AA}$ $\text{ZnO}/\text{Be}_x\text{Mg}_y\text{Zn}_{1-x-y}\text{O}$ quantum well oriented in polar and semipolar axes. Figure.4 shows the results as a function of y for several chosen values of x . The panels (a) and (b) are for the quantum wells oriented in the polar and semipolar axes, respectively, in the case I. F_{bi} for the polar quantum wells becomes large in magnitude with the increasing Be concentration in accordance with the panel (a) of Figure.3. The magnitude of F_{bi} exceeds 8 MV cm^{-1} . The quantum wells oriented in the semipolar axis has F_{bi} values in magnitude nearly a quarter of those shown in the panel (b). Particularly, the values become positive, in other words, F_{bi} changes direction in the semipolar orientation. Indeed this is a consequence of the sign reversal of the polarization difference at the well-barrier interface as shown in the panel (b) of Figure.3. Note that F_{bi} becomes almost zero for $x = 0$ as shown by the blue solid line in the panel. The field values are less sensitive to the changes in the Mg concentration for both orientations. The results of the calculations carried out for the case II are depicted in the panels (a) and (b) for the polar and semipolar orientations, respectively. The case II, that is the case of thin barrier layers strained on the substrate, leads to the F_{bi} values reduced in magnitude for both orientations. The main reason behind this is the decreasing barrier width (Harrison and Valavanis, 2016). A consequence of making the barriers thinner is that the built-in electric field inside the barrier layer increases in magnitude.

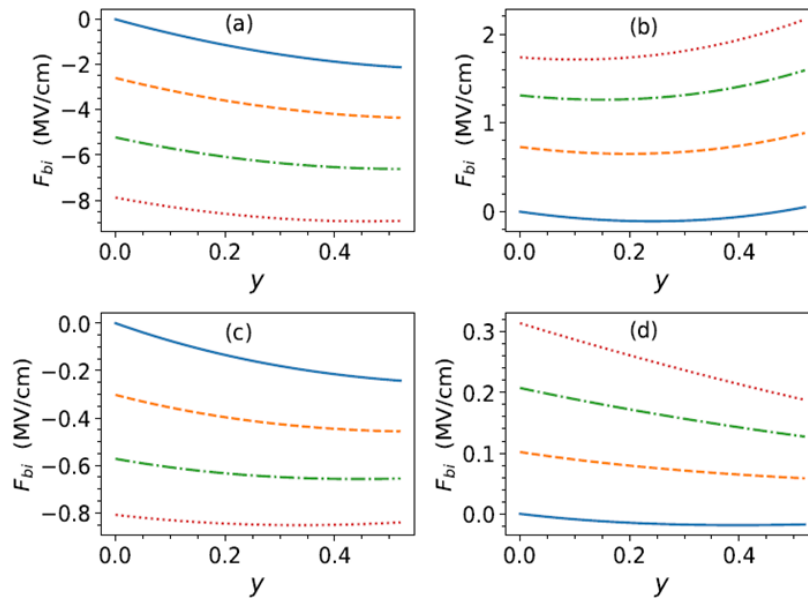


Figure.4. The built-in electric field inside the well layer of a $30 - \text{\AA}$ ZnO/Be_xMg_yZn_{1-x-y}O quantum well in the case of the relaxed barrier layer: (a) when the growth axis is the polar axis and (b) the semipolar axis. The built-in electric field inside the well layer of a $30 - \text{\AA}$ ZnO/Be_xMg_yZn_{1-x-y}O quantum well in the case of the strained barrier layer: (c) when the growth axis is the polar axis and (d) the semipolar axis. The solid, dashed, dashed-dotted, and dotted lines stand for $x = 0, 0.06, 0.12, \text{ and } 0.18$, respectively, in all panels

Nonpolar quantum wells

The bending of the potential energy profile by the built-in electric field inside the wurtzite quantum well structures introduces undesired results regarding their optical and electrical properties (Feezell et al., 2013; Monavarian et al., 2018; Yıldırım, 2021). The arising triangular potential energy profile around the well region may cause an ISBT energy for the conduction band electrons persistent around a value despite the increasing well width. The distortion of the wave functions by the field reduces their overlaps and therefore yields a smaller oscillator strength (Feezell et al., 2013; Monavarian et al., 2018; Yıldırım, 2021). To eliminate these effects, quantum well structures grown in a nonpolar orientation have been suggested (Meng et al., 2019).

While such a growth removes the built-in electric field, the layers in the structure can be strained. Therefore, it is necessary to discuss the amount of the strain in the layers in this orientation. The lattice constant of the binary BeO is much less than those of the binaries MgO and ZnO. Therefore, a compressive strain is expected inside a ZnO well layer when it is grown on a relaxed Be_xMg_yZn_{1-x-y}O barrier layer (that is, the case I). Figure.5 depicts the nonzero components of the strain tensor ϵ_{xx} , ϵ_{yy} and ϵ_{zz} inside the ZnO well layer as a function of the Be and Mg concentrations when the structure has a nonpolar growth. The calculated in-plane strains are negative and they grow in magnitude especially as x becomes larger. The ϵ_{yy} values are generally greater in magnitude than the ϵ_{xx} values. ϵ_{yy} reaches to the values as large as 5% in magnitude. However, the out-of plane component, ϵ_{zz} , is positive but it also goes up as both concentration values increase. It is around 4% at maximum. The calculated strain values are greater than in magnitude those inside nonpolar ZnCdO/ZnO quantum wells (Yıldırım, 2021).

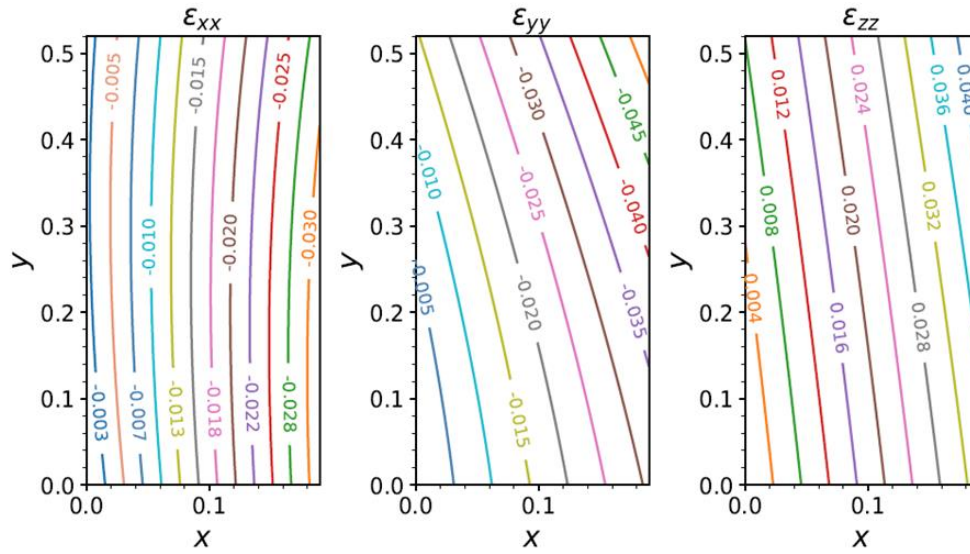


Figure.5. Strain components as a function of the concentrations, x and y , in a ZnO well layer grown on a relaxed $\text{Be}_x\text{Mg}_y\text{Zn}_{1-x-y}\text{O}$ barrier layer in nonpolar orientation

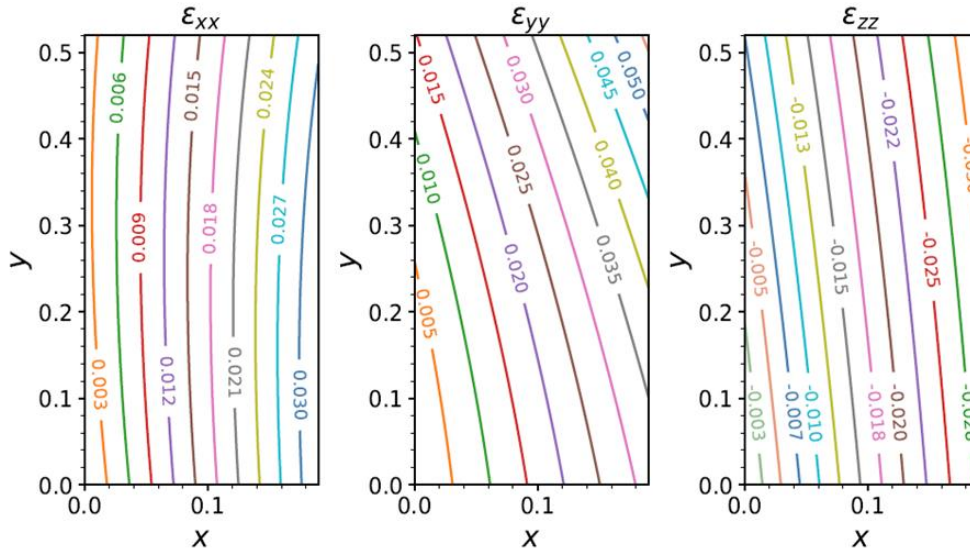


Figure.6. Strain components as a function of the concentrations, x and y , in a $\text{Be}_x\text{Mg}_y\text{Zn}_{1-x-y}\text{O}$ barrier layer strained on a ZnO substrate in nonpolar orientation

The ZnO well layers do not have any strain in the case II. However, the thin BeMgZnO barrier layers are strained on the ZnO substrate. The results of the calculations of the strain inside the barrier layers in this case are plotted in Figure.6 as a function of the Be and Mg concentrations. The strain components have opposite signs compared to those shown in Figure.5. As for their magnitudes, the in-plane strains are comparable but the out-of plane component, ϵ_{zz} , is smaller. Consequences of the calculated strains in both cases, that is the cases I and II, for the energy band gap and therefore the conduction band off set are taken into account, when the ISBT energies in the nonpolar quantum wells of ZnO/BeMgZnO are computed.

The ISBT energies of the conduction band electrons in the nonpolar ZnO/ $\text{Be}_x\text{Mg}_y\text{Zn}_{1-x-y}\text{O}$ quantum wells are calculated by applying the effective mass and envelope function approximations. Within these approximations (Harrison and Valavanis, 2016), the Hamiltonian of an electron can be expressed as:

$$H = -\frac{\hbar^2}{2} \frac{\partial}{\partial z} \frac{1}{m^*(z)} \frac{\partial}{\partial z} + V(z) + V_s(z) - e\phi(z) + V_{xc}(z) \quad (1)$$

where $V(z)$ is the conduction band offset, which is given by 67.5% of the difference between the band gaps of the well and barrier layers (Meng et al., 2019), $\varphi(z)$ is the electrostatic potential due to the free and bound charges, $V_s(z)$ is the strain-induced shift in the conduction band edge (Harrison and Valavanis, 2016), and V_{xc} is the exchange-correlation energy (Helm, 1999).

There are few works on the band gap of the quaternary compound (Toporkov et al., 2016; Zhao et al., 2018)), BeMgZnO. According to DFT calculations given in Ref. (Toporkov et al., 2016), the band gap and lattice constants of the quaternary alloy non-linearly depend on the concentrations of its binary alloys. That is, the band gap, E_g and the lattice constants, a_0 and c_0 , of the quaternary compound $Be_xMg_yZn_{1-x-y}O$ are formulated as (Toporkov et al., 2016).

$$\begin{aligned} A(Be_xMg_yZn_{1-x-y}O) \\ = xA(BeO) + yA(MgO) + (1-x-y)A(ZnO) - b_{BeZnO}x(1-x) \\ - b_{MgZnO}y(1-y) - b_{xy}xy \end{aligned} \quad (2)$$

where A is either of the quantities, b_{BeZnO} , b_{MgZnO} and b_{xy} are the bowing parameters for the related quantity. Equation (2) is in good agreement with the outcomes of the experimental studies on the MBE grown quaternary BeMgZnO thin films up to $x = 0.19$ and $y = 0.52$ (Toporkov et al., 2016). The bowing parameters are listed in Table 2.

The strain-induced shift in the conduction band edge is calculated through the following expression (Harrison and Valavanis, 2016):

$$V_s(z) = (\epsilon_{xx} + \epsilon_{yy})a_{ct} + \epsilon_{zz}a_{cz} \quad (3)$$

where a_{ct} and a_{cz} are the conduction band deformation potentials in the directions perpendicular and parallel to the growth axis, respectively.

The electrostatic potential is computed through the Poisson equation:

$$\frac{d}{dz} \epsilon_0 \epsilon(z) \frac{d}{dz} \varphi(z) = e[n(z) - N_D^+(z)] \quad (4)$$

where ϵ is the static dielectric constant, $n(z)$ and N_D^+ are the electron and ionized donor densities, respectively (Gunna et al., 2007).

The intersubband absorption spectrum of the quantum well is influenced by the many-body effects, such that a peak in the spectrum does not occur at the bare ISBT energy E_{ij} , where i and j stand for the subband index, but it shifts to an energy given by (Gunna et al., 2007):

$$\tilde{E}_{ij} = E_{ij} \sqrt{1 + \alpha_{ij} - \beta_{ij}} \quad (5)$$

where $i > j$. The quantities α_{ij} and β_{ij} are known as the the depolarization and excitonic shift parameters (Gunna et al., 2007), respectively. These parameters can be computed through the expressions given by (Gunna et al., 2007):

$$\alpha_{ij} = \frac{2e^2 \Delta n_s}{\epsilon_0 \epsilon_s E_{ij}} \int_{-\infty}^{\infty} dz \left[\int_{-\infty}^z dz' \phi_i(z') \phi_j(z') \right]^2 \quad (6)$$

and

$$\beta_{ij} = \frac{2 \Delta n_s}{E_{ij}} \int_{-\infty}^{\infty} dz |\phi_i(z)|^2 |\phi_j(z)|^2 \frac{\partial V_{xc}[n(z)]}{\partial n(z)} \quad (7)$$

where Δn_s represents the areal electron concentration difference between the corresponding energy states, and $\phi_i(z)$ is the wave function of the i th subband.

Equations (1) and (4) are self-consistently solved by using an iterative method based on a predictor-corrector approach (Gunna et al., 2007) following their discretization through finite differences.

RESULTS AND DISCUSSION

We have calculated the potential energy profile of a nonpolar 30 – Å ZnO/Be_{0.18}Mg_{0.25}Zn_{0.57}O quantum well, uniformly doped to $1 \times 10^{25} m^{-3}$, in the cases I and II. Figure.7 (a) depicts the potential energy profile in the case I. The squared wave functions of the ground and the first excited states are also plotted in the same graph. Since the well layer is narrow, the quantum well admits only two bound states. The ISBT energy between them is 317 meV, but it becomes 319 meV following the addition of the many-body effects. The panel (b) of the same figure presents the plot of the potential energy profile in the case II. The barrier is 70 Å in width. With the introduction of the much thinner barrier layer, ISBT energy between the subband states drop to $E_{21} = 308$ meV and $\tilde{E}_{21} = 306$ meV. That is, nearly a 10 meV-change in the energies occurs. However, one important consequence of the making the barrier layer thinner is that a set of quasibound states (not shown) are introduced to the regions before the left barrier and after the right barrier.

Figure.8 depicts the ISBT energies between the subbands in nonpolar ZnO/Be_xMg_{0.75}Zn_{0.75-x}O quantum wells, uniformly doped to $1 \times 10^{25} m^{-3}$, as a function of the well width L_W in the case I. The lowest three subbands are considered: the panel (a) shows the transition energies between the ground and the first excited states, while the panel (b) shows those between the first and second excited states. Three different values of the Be concentration are applied: 0.045, 0.09 and 0.18. The solid lines stand for the energies when the depolarization and the excitonic shift parameters are included into the calculations. The contribution of the parameters becomes important as the quantum well becomes wider. These parameters provide less than 10% fractional change when $L_W \leq 40$ Å for E_{21} and when $L_W \leq 70$ Å for E_{32} . It is obvious that these parameters will contribute more if the doping level increases. In terms of wavelength, the calculated transition energies are between around 3.1 and 24.8 μm for E_{21} and between around 4.13 and 13.8 μm for E_{32} , in other words; they fall into the mid-infrared region of the light.

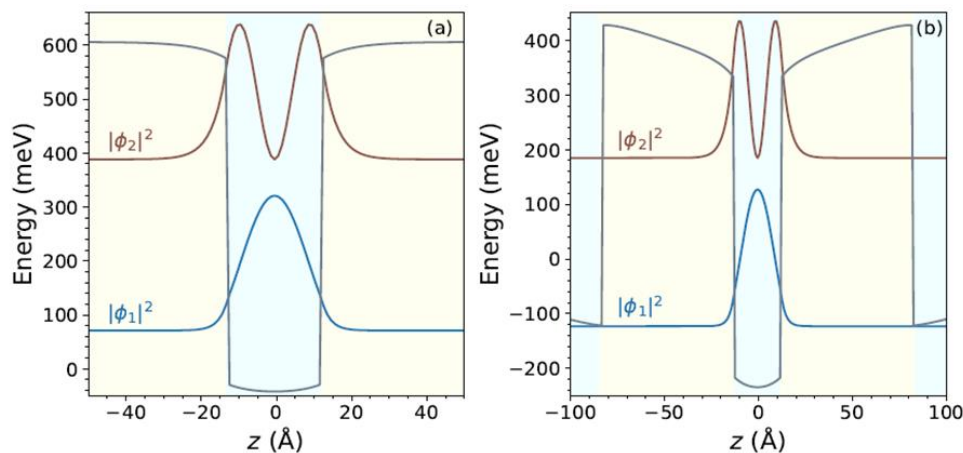


Figure.7. The potential energy profile of a nonpolar 25 – Å ZnO/Be_{0.18}Mg_{0.25}Zn_{0.57}O quantum well together with the squared wave functions of its ground and first excited subbands: (a) The case of the relaxed barrier layer and (b) the case of the strained barrier layer. The squared wave functions are positioned at their respective subband energies. The well region is assumed to be uniformly doped to $1 \times 10^{25} m^{-3}$

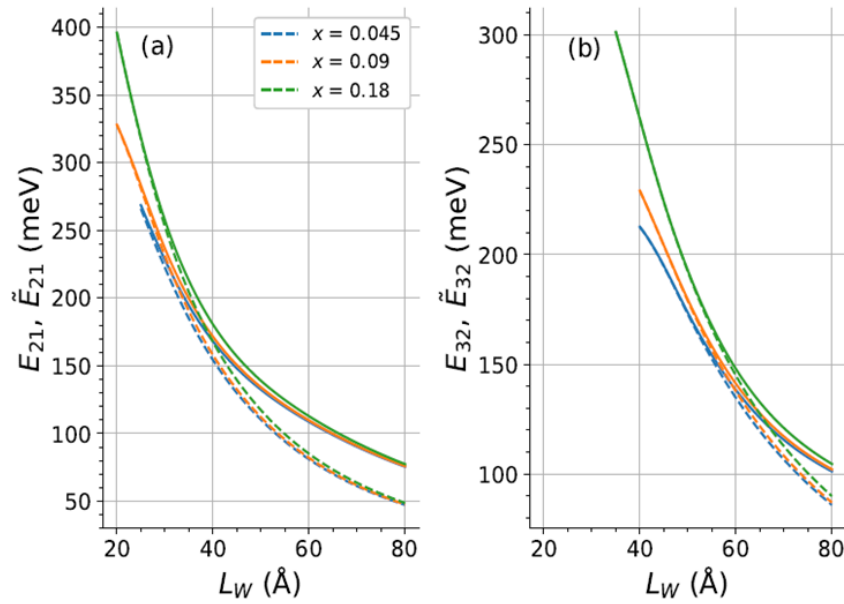


Figure.8. Intersubband transition energies between the ground and the first two excited states in nonpolar ZnO/Be_xMg_{0.25}Zn_{0.75-x}O quantum wells as a function of the well width, L_W . The barrier layer is relaxed. Solid lines indicate the transition energies following the addition of the depolarization and excitonic shift parameters

The band gap of the nonpolar ZnO/Be_xMg_yZn_{1-x-y}O quantum well depends on the Mg concentration as well as the Be concentration. Figure.9 displays the ISBT energies between the subbands of the quantum well in the case I. Three different values of the Mg concentration (0.125, 0.25 and 0.5) are considered while x is kept fixed at 0.18. The solid lines stand for the transition energies when the depolarization and excitonic shift parameters are included into the calculations. The narrow quantum wells, such that $L_W \leq 40 \text{ \AA}$, do not admit a first excited state at low y values. As the y value increases, the E_{21} intersubband transition energy goes up to 700 meV. The contribution of the many-body effects to the ISBT energies becomes less important as the wells become narrow as in the previous calculations, shown in Figure.6. The available ISBT energies lie between nearly 1.77 and $24.8 \mu\text{m}$ in terms of wavelength, or they fall into far- and mid-infrared regions of the light.

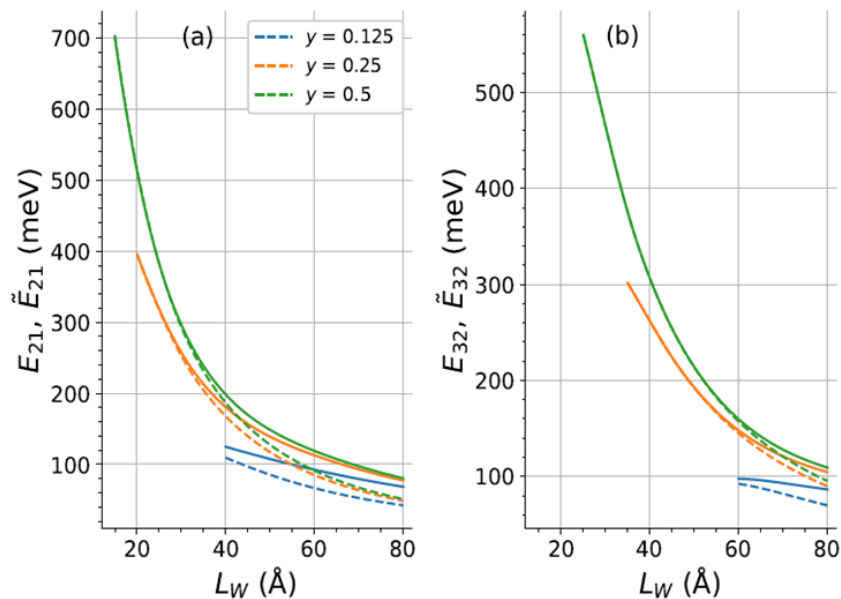


Figure.9. Intersubband transition energies between the ground and the first two excited states in nonpolar ZnO/Be_{0.18}Mg_yZn_{0.82-y}O quantum wells as a function of the well width, L_W . The barrier layer is relaxed. Solid lines indicate the transition energies following the addition of the depolarization and excitonic shift parameters

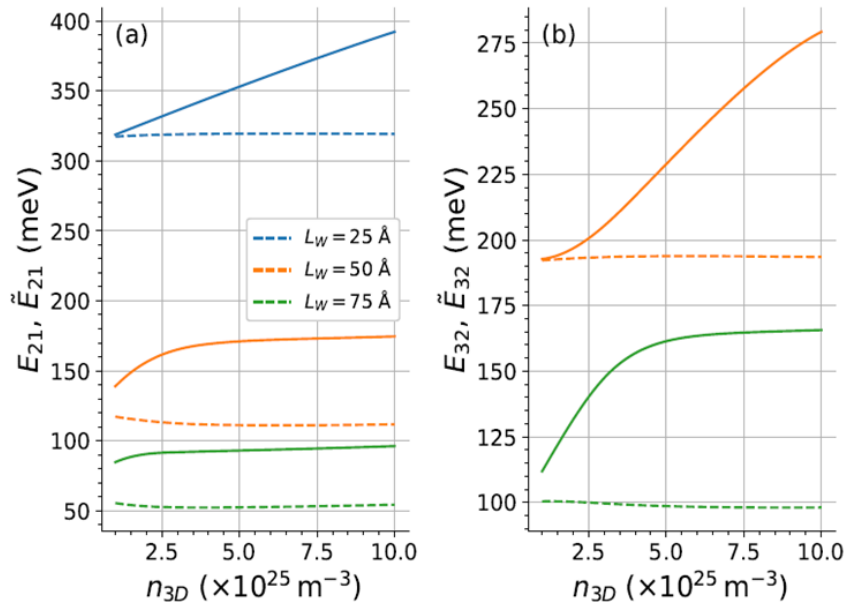


Figure.10. Intersubband transition energies between the ground and the first two excited states in nonpolar ZnO/Be_{0.18}Mg_{0.25}Zn_{0.57}O quantum wells as a function of the doping level of the well layer, n_{3D} . The barrier layer is relaxed. Solid lines indicate the transition energies following the addition of the depolarization and excitonic shift parameters

The doping level inside the well layer has an obvious effect on the transition energies. To see the extent of the effect, the calculated ISBT energies are plotted against the doping level in Figure.10 for three different values of the well width in the case I: 25, 50, and 75 Å. As in the previous plots, the solid lines indicate those energies including the depolarization and the excitonic shift parameters. The ISBT energies, E_{21} and E_{32} , change very little (a few meV) with the increasing doping level. However, the modified ISBT energies, \tilde{E}_{21} and \tilde{E}_{32} , deeply depend on the doping level. It is clear that the parameters contribute to the transition energies much more in the case of a wide well. For instance, the fractional changes in E_{21} are 23, 55, and 78% in the increasing order of the well width. These numbers for E_{32} drop to 44 and 69% for $L_W = 50$ and 75 Å.

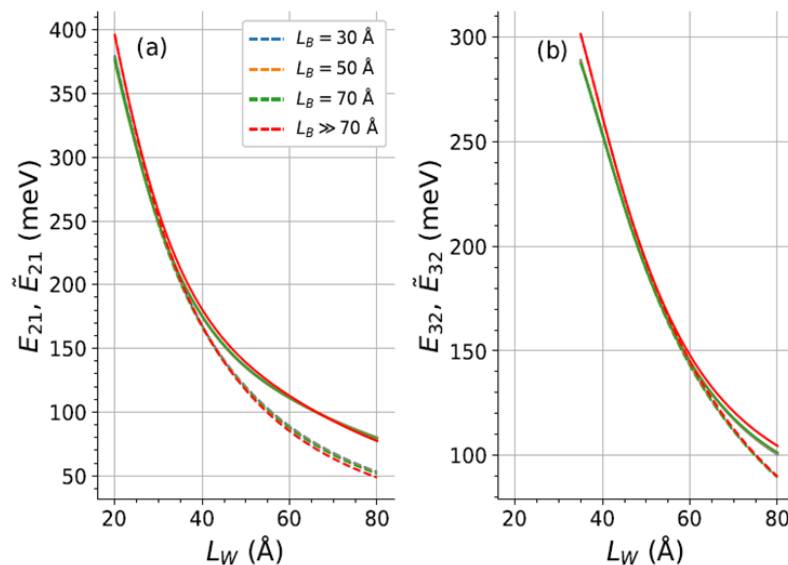


Figure.11. Intersubband transition energies between the ground and the first two excited states in nonpolar ZnO/Be_{0.18}Mg_{0.25}Zn_{0.57}O quantum wells as a function of the well width, L_W . The barrier layer is strained on a ZnO substrate. Red lines indicate calculations for the same quantum well with relaxed barrier. L_B is for the thickness of the barrier layer. Solid lines indicate the transition energies following the addition of the depolarization and excitonic shift parameters

Figure.11 depicts the ISBT energies ZnO/Be_{0.18}Mg_{0.25}Zn_{0.57}O quantum wells against L_W for several values of the barrier width, L_B , in the case II. Figure.11 also includes the result of the ZnO/Be_{0.18}Mg_{0.25}Zn_{0.57}O quantum wells of the case I shown by red lines for comparison. L_B has three different values: 30, 50, and 70 Å. The ISBT energies do not change appreciably for the thinner barriers. However, the wave functions belonging to the subbands higher than the ground state start to penetrate to the barrier and even further as the barrier becomes thinner.

The present calculations indicate in principle that nonpolar ZnO/BeMgZnO quantum wells may have a contribution to the area of the optoelectronic devices based on ISBTs and working in the far- and mid-infrared regions, together with other ZnO-based heterostructures. However, it should be mentioned that both experimental and theoretical works on BeMgZnO quantum wells, oriented in polar, semipolar or nonpolar axis, are lacking. Hence the results in the current work need a comparison with experimental outcomes and further theoretical calculations and thus a confirmation.

CONCLUSION

We have calculated the polarization properties of ZnO well and Be_xMg_yZn_{1-x-y}O barrier layers in their polar and semipolar quantum wells up to $x = 0.19$ and $y = 0.52$. The intersubband transition (ISBT) energies of the electrons within the conduction band of the nonpolar quantum wells have been mainly aimed in the current study. The Schrödinger and Poisson equations for the ZnO/Be_xMg_yZn_{1-x-y}O quantum well structures have been solved self-consistently by using an iterative method based on a predictor corrector approach. It has been shown that polar and semipolar ZnO/BeMgZnO quantum wells suffer from strong built-in electric field inside the well layer because of the polarization components of the layers. The field values can be greater than 8 MV/cm in magnitude. Applying thinner barrier layers reduces the built-in electric field inside the well layer by one order of magnitude, but makes the built-in electric field inside the barrier layer greater in magnitude. On the other hand, the nonpolar ZnO/BeMgZnO quantum wells do not have built-in electric field and admit square potential energy profiles. They allow ISBT energies in the far- and mid-infrared regions. The critical thickness considerations of the BeMgZnO barrier layer on a ZnO substrate yields thickness values as low as 65 Å. While such thin BeMgZnO barrier layers provide similar ISBT energies, they create quasibound states outside the well layer. We believe that the results of the present study will be helpful to researchers in designing possible quantum optoelectronic devices of nonpolar ZnO/BeMgZnO quantum wells based on the ISBTs and working in the far- and mid-infrared regions.

Çıkar Çatışması

The article authors declare that there is no conflict of interest between them.

Author's Contributions

The authors declare that they have contributed equally to the article.

REFERENCES

- Ding K, Avrutin V, Izioumskaia N, Ullah MB, Özgür Ü, Morkoç H, 2018. Fabrication of Schottky Diodes on Zn-polar BeMgZnO/ZnO Heterostructure Grown by Plasma-Assisted Molecular Beam Epitaxy. *Journal of Visualized Experiments*, 140: 58113. doi:<https://dx.doi.org/10.3791/58113>
- Duan Y, Qin L, Tang G, Shi L, 2008. First-Principles Study of Ground- and Metastable-State Properties of XO (X = Be, Mg, Ca, Sr, Ba, Zn and Cd). *The European Physical Journal B*, 66: 201-209. doi:<https://doi.org/10.1140/epjb/e2008-00415-3>

- Duman S, Sütlü A, Bağcı S, Tütüncü HM, Srivastava GP, 2009. Structural, Elastic, Electronic, and Phonon Properties of Zinc-Blende and Wurtzite BeO. *Journal of Applied Physics*, 105: 033719. doi:<https://doi.org/10.1063/1.3075814>
- Feezell D, Sharma Y, Krishna S, 2013. Optical Properties of Nonpolar III-Nitrides for Intersubband Photodetectors. *Journal of Applied Physics*, 113: 133103. doi:<https://doi.org/10.1063/1.4798353>
- Grundmann M, Zúñiga-Pérez J, 2015. Pseudomorphic ZnO-Based Heterostructures: From Polar Through All Semipolar to Nonpolar Orientations. *Physica Status Solidi B*, 253: 351-360. doi:<https://doi.org/10.1002/pssb.201552535>
- Gunna S, Bertazzi F, Paiella R, Bellotti E, 2007. Intersubband Absorption in AlGaIn/GaN Quantum Wells. J. Piprek, in: J. Piprek (Ed.), *Nitride Semiconductor Devices: Principles and Simulation*. Wiley-VCH, pp 117-143, Weinheim. doi:<https://doi.org/10.1002/9783527610723.ch6>
- Harrison P, Valavanis A, 2016. *Quantum Wells, Wires and Dots: Theoretical and Computational Physics of Semiconductor Nanostructures*, 4th ed., John Wiley and Sons, Malaysia. doi:<https://doi.org/10.1002/9781118923337>
- Helm M, 1999. The Basic Physics of Intersubband Transitions. H. C. Liu, and F. Capasso, in: *Intersubband Transitions in Quantum Wells Physics*. Academic Press, 62: pp 1-99, San Diego. doi:[https://doi.org/10.1016/S0080-8784\(08\)60304-X](https://doi.org/10.1016/S0080-8784(08)60304-X)
- Holec D, Costa, PMFJ, Kappers MJ, Humphreys CJ, 2007. Critical Thickness Calculations for InGaIn/GaN. *Journal of Crystal Growth*, 303: 314-317. doi:<https://doi.org/10.1016/j.jcrysgro.2006.12.054>
- Hong W-P, Park S-H, 2021. Linewidth Enhancement Factor of Hybrid Green InGaIn/MgZnO Quantum Well Structures. *Physica E: Low-dimensional Systems and Nanostructures*, 130: 114678. doi:<https://doi.org/10.1016/j.physe.2021.114678>
- Jang S-H, Chichibu SF, 2012. Structural, Elastic, and Polarization Parameters and Band Structures of Wurtzite ZnO and MgO. *Journal of Applied Physics*, 112: 073503. doi:<https://doi.org/10.1063/1.4757023>
- Lange M, Dietrich CP, Brachwitz K, Stölzel M, Lorenz M, Grundmann M, 2011. Visible Emission from ZnCdO/ZnO Multiple Quantum Wells. *Physica Status Solidi - Rapid Research Letters*, 6(1), 31-33. doi:<https://doi.org/10.1002/pssr.201105489>
- Liu Y, Wang P, Guo L, Chen H, Yang H, 2019. Investigation of Intersubband Transition Optical Absorption in Zn_{1-x}Mg_xO/MgO/ZnO Heterostructures. *Superlattices and Microstructures*, 125: 26-33. doi:<https://doi.org/10.1016/j.spmi.2018.10.015>
- Meng B, Hinkov B, Biavan NML, Hoang HT, Lefebvre D, Hugues M, Stark D, Franckić M, Torres-Pardo A, Tamayo-Arriola J, Bajo MM, Hierro A, Strasser G, Faist J, Chauveau JM, 2021. Terahertz Intersubband Electroluminescence from Nonpolar m-Plane ZnO Quantum Cascade Structures. *ACS Photonics*, 8(1): 343-349. doi:<https://doi.org/10.1021/acsp Photonics.0c01641>
- Meng B, Tamayo-Arriola J, Le Biavan N, Bajo MM, Torres-Pardo A, Hugues M, Lefebvre D, Hierro A, Chauveau JM, Faist J, 2019. Observation of Intersubband Absorption in ZnO Coupled Quantum Wells. *Physical Review Applied*, 12: 054007. doi:<https://doi.org/10.1103/PhysRevApplied.12.054007>
- Monavarian M, Rashidi A, Feezell D, 2018. A Decade of Nonpolar and Semipolar III-Nitrides: A Review of Successes and Challenges. *Physica Status Solidi A*, 216(1): 1800628. doi:<https://doi.org/10.1002/pssa.201800628>

- Orphal L, Kalusniak S, Benson O, Sadofev S, 2017. Tunable Intersubband Transitions in ZnO/ZnMgO Multiple Quantum Wells in the Mid Infrared Spectral Range. *AIP Advances*, 7: 115309. doi:<https://doi.org/10.1063/1.4998805>
- Özgür Ü, Alivov YI, Liu C, Teke A, Reshchikov MA, Doğan S, Avrutin V, Cho S-J, Morkoç H, 2005. A Comprehensive Review of ZnO Materials and Devices. *Journal of Applied Physics*, 98: 041301. doi:<https://doi.org/10.1063/1.1992666>
- Özgür Ü, Avrutin V, Morkoç H, 2018. Zinc Oxide Materials and Devices Grown by Molecular Beam Epitaxy. H. Mohamed, in: *Molecular Beam Epitaxy From Research to Mass Production*, Elsevier, pp343-375. doi:<https://doi.org/10.1016/B978-0-12-812136-8.00016-5>
- Park D-S, Krupski A, Sanchez AM, Choi C-J, Yi M-S, Lee H-H, McMitchell SRC, McConville CF, 2014. Optimal Growth and Thermal Stability of Crystalline Be_{0.25}Zn_{0.75}O alloy films on Al₂O₃(0001). *Applied Physics Letters*, 104: 141902. doi: <https://doi.org/10.1063/1.4870533>
- Park S-H, 2020. Cd Content Dependence of in-Plane Optical Polarization in Anisotropically Strained c-Plane CdZnO/ZnO Quantum Wells. *Physica B: Condensed Matter*, 596: 412393. doi:<https://doi.org/10.1016/j.physb.2020.412393>
- Pearnton SJ, Ren F, 2014. Advances in ZnO-Based Materials for Light Emitting Diodes. *Current Opinion in Chemical Engineering*, 3: 51-55. doi:<https://doi.org/10.1016/j.coche.2013.11.002>
- Pietrzyk MA, Wierzbicka A, Zielony E, Pieniazek A, Szymon R, Placzek-Popko E, 2020. Fundamental Studies of ZnO Nanowires with ZnCdO/ZnO Multiple Quantum Wells Grown for Tunable Light Emitters. *Sensors and Actuators A: Physical*, 315: 112305. doi:<https://doi.org/10.1016/j.sna.2020.112305>
- Prodhomme P-Y, Beya-Wakata A, Bester G, 2013. Nonlinear Piezoelectricity in Wurtzite Semiconductors. *Physical Review B*, 88: 121304(R). doi:<https://doi.org/10.1103/PhysRevB.88.121304>
- Romanov AE, Baker TJ, Nakamura S, Speck JS, 2006. Strain-Induced Polarization in Wurtzite III-Nitride Semipolar Layers. *Journal of Applied Physics*, 100: 023522. doi:<https://doi.org/10.1063/1.2218385>
- Ryu Y, Lee T-S, Lubguban JA, White HW, Kim B-J, Park Y-S, Youn C-J, 2006. Next Generation of Oxide Photonic Devices: ZnO-Based Ultraviolet Light Emitting Diodes. *Applied Physics Letters*, 88: 241108. doi: <https://doi.org/10.1063/1.2210452>
- Sadofev S, Kalusniak S, Puls J, Schäfer P, Blumstengel S, Henneberger F, 2007. Visible-Wavelength Laser Action of ZnCdO(Zn,Mg)O Multiple Quantum Well Structures. *Applied Physics Letters*, 91: 231103. doi:<https://doi.org/10.1063/1.2822889>
- Schleife A, Fuchs F, Rödl C, Furthmüller J, Bechstedt F, 2009. Band-Structure and Optical-Transition Parameters of Wurtzite MgO, ZnO, and CdO from Quasiparticle Calculations. *Physica Status Solidi B*, 246(9): 2150-2153. doi:<https://doi.org/10.1002/pssb.200945204>
- Shein IR, Kīko VS, Makurin YN, Gorbunova MA, Ivanovskī AL, 2007. Elastic Parameters of Single-Crystal and Polycrystalline Wurtzite-Like Oxides BeO and ZnO: Ab Initio Calculations. *Physics of the Solid State*, 49: 1067–1073. doi:<https://doi.org/10.1134/S106378340706008X>
- Shteplyuk I, Khranovskyy V, Yakimova R, 2015. Effect of Zn–Cd Interdiffusion on the Band Structure and Spontaneous Emission of ZnO/Zn_{1-x}Cd_xO/ZnO Quantum Wells. *Superlattices and Microstructures*, 85: 438-444. doi:<https://doi.org/10.1016/j.spmi.2015.06.013>
- Sirkeli VP, Hartnagel HL, 2019. ZnO-Based Terahertz Quantum Cascade Lasers. *Opto-Electronics Review*, 27(2): 119-122. doi:<https://doi.org/10.1016/j.opelre.2019.04.002>

- Toporkov M, Avrutin V, Okur S, Izyumskaya N, Demchenko D, Volk J, Smith DJ, Morkoç H, Özgür Ü, 2014. Enhancement of Be and Mg Incorporation in Wurtzite Quaternary BeMgZnO Alloys with up to 5.1 eV Optical Bandgap. *Journal of Crystal Growth*, 402: 60-64. doi:<https://doi.org/10.1016/j.jcrysgro.2014.04.028>
- Toporkov M, Demchenko DO, Zolnai Z, Volk J, Avrutin V, Morkoç H, Özgür Ü, 2016. Lattice Parameters and Electronic Structure of BeMgZnO Quaternary Solid Solutions: Experiment and Theory. *Journal of Applied Physics*, 119: 095311. doi:<https://doi.org/10.1063/1.4942835>
- Ullah MB, 2017. Growth of Zn-Polar BeMgZnO/ZnO Heterostructure with Two Dimensional Electron Gas (2DEG) and Fabrication of Silver Schottky Diode on BeMgZnO/ZnO Heterostructure. Virginia Commonwealth University, Richmond. doi:<https://doi.org/10.25772/SKM4-5149>
- Ullah MB, Ding K, Nakagawara T, Avrutin V, Özgür Ü, Morkoç H, 2017. Characterization of Ag Schottky Barriers on Be_{0.02}Mg_{0.26}ZnO/ZnO Heterostructures. *Physica Status Solidi – Rapid Research Letters*, 12(2): 1700366. doi:<https://doi.org/10.1002/pssr.201700366>
- Wagner MR, Callsen G, Reparaz JS, Kirste R, Hoffmann A, Rodina AV, Schleife A, Bechstedt F, Phillips MR, 2013. Effects of Strain on the Valence Band Structure and Exciton-Polariton Energies in ZnO. *Physical Review B*, 88: 235210. doi:<https://doi.org/10.1103/PhysRevB.88.235210>
- Xu Y-N, Ching WY, 1993. Electronic, Optical, and Structural Properties of Some Wurtzite Crystals. *Physical Review B*, 48: 4335. doi:<https://doi.org/10.1103/PhysRevB.48.4335>
- Yan Q, Rinke P, Winkelkemper M, Qteish A, Bimberg D, Scheffler M, van de Walle CG, 2012. Strain Effects and Band Parameters in MgO, ZnO, and CdO. *Applied Physics Letters*, 101: 152105. doi:<https://doi.org/10.1063/1.4759107>
- Yıldırım H, 2021. Non-polar ZnCdO/ZnO Step-Barrier Quantum Wells Designed for THz Emission. *Photonics and Nanostructures - Fundamentals and Applications*, 43: 100859. doi:<https://doi.org/10.1016/j.photonics.2020.100859>
- Yildirim H, 2019. Nonlinear Optical Absorption in Wurtzite ZnCdO Quantum Wells. *Materials Research Express*, 6: 0850g9. doi:<https://doi.org/10.1088/2053-1591/ab28d2>
- Zhang T, Li M, Chen J, Wang Y, Miao L, Lu Y, He Y, 2022. Multi-Component ZnO Alloys: Bandgap Engineering, Hetero-Structures, and Optoelectronic Devices. *Materials Science and Engineering: R: Reports*, 147: 100661. doi:<https://doi.org/10.1016/j.mser.2021.100661>
- Zhao C-Z, Sun S-Y, Sun X-D, Wang S-S, Wang J, 2018. The Band Gap Energy of Be_xMg_yZn_{1-x-y}O Calculated by Modified Simplified Coherent Potential Approximation. *Superlattices and Microstructures*, 11:, 255-260. doi:<https://doi.org/10.1016/j.spmi.2017.11.003>
- Zhao K, Chen G, Hernandez J, Tamargo MC, Shen A, 2015. Intersubband Absorption in ZnO/ZnMgO Quantum Wells Grown by Plasma-Assisted Molecular Beam Epitaxy on c-Plane Sapphire Substrates. *Journal of Crystal Growth*, 425: 221-224. doi:<https://doi.org/10.1016/j.jcrysgro.2015.02.002>
- Zúñiga-Pérez J, 2017. ZnCdO: Status After 20 Years of Research. *Materials Science in Semiconductor Processing*, 69: 36-43. doi:<https://doi.org/10.1016/j.mssp.2016.12.002>